Identification and Sensorless Control Using Embedded System of PMSM Based on FOC Strategy and Power Factor Correction

Claudiu-Ionel Nicola[*,†], Marcel Nicola[*], Dumitru Sacerdoțianu[*], Sebastian Popescu[*] and Adrian Vintilă[*]

[*] National Institute for Research, Development and Testing in Electrical Engineering – ICMET / Research Department, Craiova, Romania, marcel_nicola@yahoo.com, dumitru_sacerdotianu@yahoo.com, tnpopescu@icmet.ro
[†] University of Craiova / Department of Automatic Control and Electronics, Craiova, Romania, claudiu@automation.ucv.ro

***Abstract* - This article presents the procedure for identifying the electrical and mechanical parameters of the PMSM (Permanent Magnet Synchronous Motor). The parameter identification procedure is required in the event that the motor's electrical and mechanical parameters are unknown, or in industrial applications at the beginning of a drive cycle due to variations of the PMSM parameters with the temperature. The parameter identification procedure is implemented in the Matlab/Simulink environment. This procedure was also implemented in an embedded system and the results of the two (offline and online) identification methods of the nominal parameters of the PMSM are presented comparatively to the parameters in the datasheet. It presents the block structure of the PFC together with the numerical simulations achieved in Matlab/Simulink, on the improvement of the PF (Power Factor) of the supply circuit. It also presents the block structures of the FOC (Field Oriented Control) strategy and of the back-EMF (back Electromotive Force) sliding mode, MRAS (Model Reference Adaptive System), and PLL (Phase Locked Loop) type observers. The numerical simulations show the superiority of rotor speed estimation when using the back-EMF sliding mode observer compared to the rotor speed estimate provided by MRAS and PLL observers.**

Cuvinte cheie: *PMSM, FOC, identificare parametri, corectare PF, observer de stare, sistem embedded.*

Keywords: *PMSM, FOC, parameters identification, PF correction, state observer, embedded system.*

I. INTRODUCTION

The ever-growing use of PMSMs in variable speed electric drives, robot operation, computer peripherals is based on the fact that these motors have low power consumption, reduced dimensions and high duty density. The generation of the magnetic field in PMSMs is carried out by permanent magnets. Low inertia and rapid response is due to the absence of the rotor cage. Some of the general advantages of PMSMs are: easy cooling, losses concentrated in the stator, low harmonic contents in the torque, and high performance of control due to the sinusoidal form of the back-EMF. By making use of the characteristics and advantages of PMSMs, algorithms and advanced control methods have been developed [1-3]. In addition to standard DTC (Direct Torque Control) and FOC control strategies [4, 5], we mention methods as robust control [6], adaptive control [7, 8], model predictive control [9], and also neuro-fuzzy and intelligent control [10].

The above mentioned control systems can acquire the speed response from special transducers or they can use software implemented observers, which allow for these transducers to be renounced, thereby providing advantages on the reliability of the global control system. Among these we mention the Kalman filters, the back-EMF sliding mode observer, the MRAS observer, and the PLL observer [11-14].

There is also a growing interest in improving the energy quality. One of the methods which are applicable to a wide range of outputs is the PFC implementation. PFC control techniques have been developed for the relatively small output range in which the PMSM is also included. These methods use the control of a transistor (MOSFET, IGBT, etc.) which connects or disconnects a series inductance at high frequencies, so that the phase shift between the current and the voltage absorbed from the power supply is zero [15-17].

The estimation and identification of the electrical and mechanical parameters of PMSM is a particular problem. As a result of the significant development of microcontroller computation power in embedded systems, complex control algorithms like those mentioned above, as well as PMSM parameter identification algorithms, are implemented in real-time systems [18-22].

This article presents the implementation of a power factor correction and a sensorless control system with FOC strategy and back-EMF observer, in an embedded system. The problem of identifying the electrical and mechanical parameters of the PMSM is also addressed, both by numerical simulations and by online identification. The rest of paper is structured as follows: the mathematical model of the PMSM is described in Section 2. Section 3 presents the estimation of the PMSM's parameters through numerical simulation. Section 4 presents the numerical simulation of the power factor correction. The comparative implementation of the back-EMF, the MRAS, and the PLL observers for the sensorless control of the PMSM is presented in Section 5. The hardware and software implementation for the sensorless control of the PMSM is presented in Section 6. The last section presents some conclusions and ideas for future works.

II. PMSM MATHEMATICAL MODEL

Following [4, 5], [26] with the usual notation, in a, b, c reference frame, and the stator voltage equations are given by:

$$\begin{bmatrix} v_a \\ v_b \\ v_c \end{bmatrix} = \begin{bmatrix} R_s & 0 & 0 \\ 0 & R_s & 0 \\ 0 & 0 & R_s \end{bmatrix} \begin{bmatrix} i_a \\ i_b \\ i_c \end{bmatrix} + \begin{bmatrix} \frac{d\psi_a}{dt} \\ \frac{d\psi_b}{dt} \\ \frac{d\psi_c}{dt} \end{bmatrix} \quad (1)$$

where v_a, v_b and v_c represents the phase voltages on each stator windings, R_s represents the phase resistance stator winding, i_a, i_b, and i_c represents the currents stator, and ψ_a, ψ_b, and ψ_c represents the magnetic flux on each stator windings.

Note with θ_e the electrical angle, θ_r rotor angle and N the number of pole pairs. With these $\theta_e = N \cdot \theta_r$.

Using the Park's transformation given by:

$$P = 2/3 \begin{bmatrix} \cos\theta_e & \cos(\theta_e - 2\pi/3) & \cos(\theta_e + 2\pi/3) \\ -\sin\theta_e & -\sin(\theta_e - 2\pi/3) & -\sin(\theta_e + 2\pi/3) \\ 1/2 & 1/2 & 1/2 \end{bmatrix} \quad (2)$$

The equations of voltages and stator currents are obtained in d-q reference frame:

$$\begin{aligned} v_d &= R_s i_d + L_d \frac{di_d}{dt} + N\omega i_q L_q \\ v_q &= R_s i_q + L_q \frac{di_q}{dt} + N\omega(i_d L_d + \psi_m) \end{aligned} \quad (3)$$

where in addition to the usual notations ψ_m represents the permanent flux linkage.

The rotor torque equations are given by:

$$\begin{aligned} T_e &= \frac{3}{2} N\left(i_q(i_d L_d + \psi_m) - i_d i_q L_q\right) \\ T_m &= T_L + B\omega + J\frac{d\omega}{dt} \end{aligned} \quad (4)$$

where J represents the rotor inertia, B represents the viscous friction coefficient, T_m represents the mechanical torque, T_e represents the electromechanical torque, and T_L represents the load torque.

The back-EMF constant k_e is defined as the maximum induced voltage by the permanent magnet in each stator phase per rotational unit:

$$k_e = N\psi_m \quad (5)$$

It results from this that the back-EMF for one phase e_{ph} can be written as follows:

$$e_{ph} = k_e\omega \quad (6)$$

The torque constant k_t is defined as the maximum torque value induced by each phase, per current unit. k_t is numerically equal to the back-EMF constant k_e when both are expressed as SI units:

$$k_t = N\psi_m \quad (7)$$

In simplified form when $L_d = L_q$ and all three phases of PMSM are balanced the electromagnetic torque T_e is given by:

$$T_e = \frac{3}{2} k_t i_q = \frac{3}{2} k_t I_{pk} \quad (8)$$

where I_{pk} represents the peak current on the winding.

From equation (8) can be obtained k_t as follows:

$$k_t = \frac{2}{3}\frac{T_e}{I_{pk}} \quad (9)$$

If in equation (9) the RMS (Root Mean Square) value $I_{line,rms}$ is used instead of the peak value on a phase I_{pk}, the torque constant k_t becomes:

$$k_t = \sqrt{\frac{2}{3}}\frac{T_e}{I_{line,rms}} \quad (10)$$

Following [4] and the equations (1) to (10) the transfer function block diagram of PMSM is presented in Fig. 1.

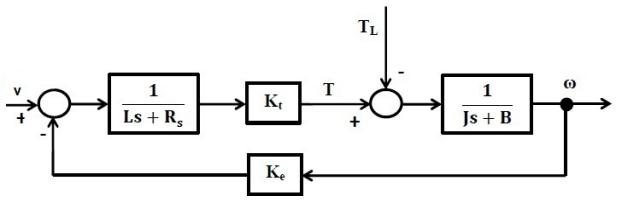

Fig. 1. The block diagram of the PMSM motor.

III. ESTIMATION OF PMSM'S PARAMETERS – NUMERICAL SIMULATION

The characteristic parameters of a PMSM specified in the previous section (winding resistance R_s, winding inductance L_s, back-EMF constant k_e, viscous damping B, inertia of rotor J, and static friction T_f), are presented in the datasheet of the PMSM. There are cases when these parameters are not known or even if they are known, due to the fact that they may vary with temperature, in industrial applications there is the question of identifying these parameters at the beginning of each drive cycle. Generally, in a drive cycle, these parameters can be considered as approximately constant during a period of time in the order of hours, and the identification procedure is in the order of tens of seconds (at least for the identification of the electrical parameters).

For a PMSM with the parameters provided in the datasheet and presented in Table 1, this section presents the estimation of these parameters by numerical simulations, and the results of the estimation of these parameters obtained by means of the online estimation procedures will be presented comparatively in the next section.

TABLE I. NOMINAL PARAMETERS OF PMSM MOTOR

Parameter	Value	Unit
Stator winding resistance Rs	0.405	Ω
Stator winding inductance: Ls	0.63e-3	H
Combined inertia of rotor and load J	4.6e-6	kg·m2

Parameter	Value	Unit
Combined viscous friction of rotor and load B	1.13e-6	N·m·s/rad
Static friction Tf	7e-4	Nm
Induced flux by the permanent magnets of the rotor in the stator phases λaf	0.175	Wb
Current at rated speed	5	A
Stall current (peak)	15.5	A
Torque at rated speed	0.185	Nm
Stall torque	0.4	Nm
back-EMF constant ke	0.0172	V/rad/s
Pole number P	8	-

Following [20], for the calculation of the winding resistance R_s and the winding inductance L_s, the stator current of the PMSM is simulated according to the mathematical model in Section 2. For a PMSM with the nominal parameters given in Table 1, the current variation is shown in Fig. 2. This is determined by applying a voltage step v_{ab} to two of the stator windings when the rotor is locked. The steady-state of the current is given by the stator resistance. The winding resistance R_s is calculated as follows:

$$R_s = \frac{1}{2}\left(\frac{v_{ab\_end}}{i_{motor\_end}}\right) \tag{11}$$

where v_{ab_end} and i_{motor_end} represents the final values in the simulation vectors for v_{ab} and i_{motor}.

The electrical time constant τ_e is obtained from Fig. 2 and represents the time when i_{motor} reaches 0.63 of the stationary value i_{motor_end}. Based on these, the winding inductance L_s is obtained as follows:

$$L_s = R_s \tau_e \tag{12}$$

Fig. 2 shows the perfect overlap of the curve representing the measured current (by the mathematical model simulation in section 2) and the estimated current given by:

$$i_{estimated} = \frac{1}{2}\left(\frac{v_{ab\_end}}{R_s}\right)\left(1 - \exp^{\tau R_s / L_s}\right) \tag{13}$$

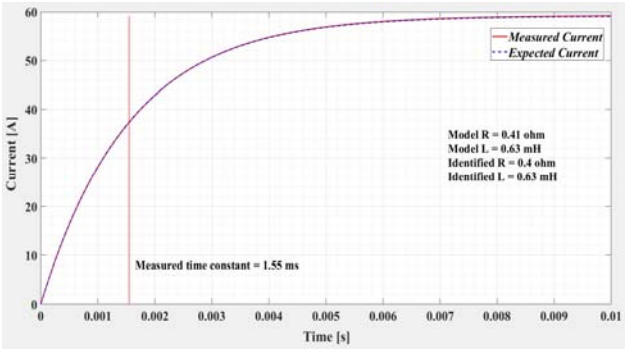

Fig. 2. Estimation of winding resistance R_s and winding inductance L_s.

Following the simulations, the following estimated values were obtained: estimated R_s=0.41Ω, τ_e=1.55ms, and L_s=0.63mH.

For the determination of the back-EMF constant k_e, the rotor is spin by a dynamometer with no electrical load. The back-EMF constant k_e can be determined from the maximum amplitude of the induced voltage. The peak line-line voltage expressed in volts can be obtained from the induced voltage (see Fig. 3):

$$v_{peak\_LL} = \max(abs(v_{ab})) \tag{14}$$

The peak line-neutral (phase) voltage can be obtained from equation (14):

$$v_{peak\_LN} = \frac{v_{peak\_LL}}{\sqrt{3}} \tag{15}$$

The back-EMF constant can be obtained for rotor angular velocity ω_{ref} expressed in rad/s:

$$k_e = \frac{v_{peak\_LN}}{\omega_{ref}} \tag{16}$$

Based on these, the estimated k_e=0.0172V/rad/s is obtained.

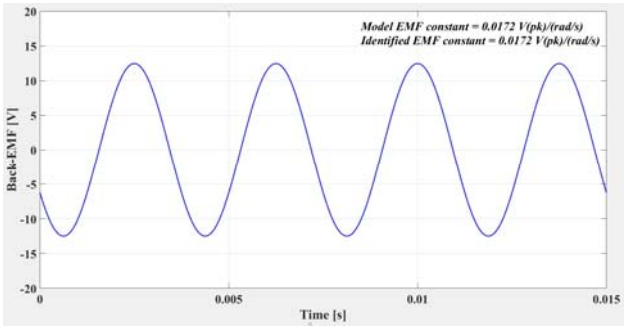

Fig. 3. Estimation of back-EMF k_e.

To determine the mechanical parameters: combined viscous friction of rotor and load B, static friction T_f, and combined inertia of rotor and load J, the motor is rotated without mechanical load. Fig. 4 shows four points distributed along the rotational speed and the calculation of the torques necessary to maintain these constant speeds. At low speeds, the required torque must overcome the static friction T_f, while at high speeds the torque must be greater than the combined viscous friction of rotor and load B. A straight line is drawn, which must run as precisely as possible through the four chosen points. The value of the torque expressed by this straight line at ω = 0 represents the static friction T_f. The slope of this line gives the combined viscous friction of rotor and load B. The results of the simulations are: estimated combined viscous friction of rotor and load B=1.1839e-06N·m·s/rad and static friction T_f=7.6476e-04Nm.

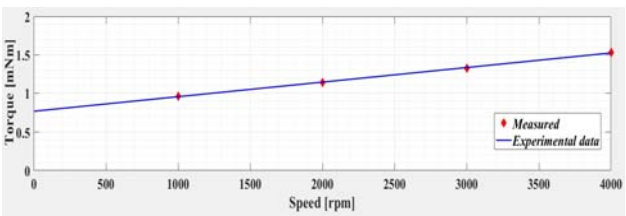

Fig. 4. Estimation of combined viscous friction of rotor and load B and static friction T_f.

For the determination of the combined inertia of rotor and load J, the reference of the electromagnetic torque is set to zero or the motor supply is interrupted. Fig. 5 shows the evolution of such a deceleration (speed run-down test). The gradient provides the deceleration, from which, together with the friction and damping torques, determines the combined inertia of rotor and load J according to equation (4). As a result of the simulations, the estimated combined inertia of rotor and load J=5.0470e-06kg·m^2 is obtained.

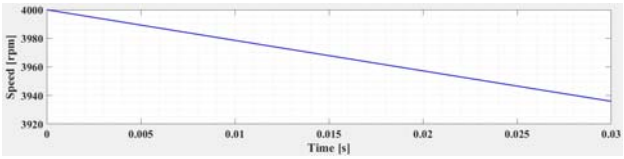

Fig. 5. Estimation of combined inertia of rotor and load J.

IV. Numerical Simulation of Power Factor Correction

A typical PMSM system operating from a single phase supply with a specialized module for PFC consists of three major stages: rectifying the input AC voltage, boosting the PFC stage, and the PMSM inverter stage. The block diagram of the system is presented in Fig. 6.

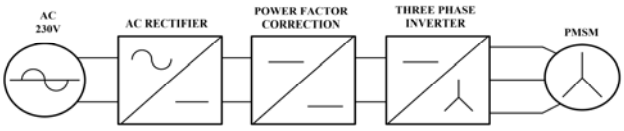

Fig. 6. The scheme for supply of PMSM, from single phase voltage.

The voltage constraint is given by:

$$u_d^2(t) + u_q^2(t) \le V_{MAX}^2 \tag{17}$$

$$V_{MAX} = \frac{V_{DC}}{\sqrt{3}} \tag{18}$$

where VDC represents the voltage of intermediate direct current circuit.

The RMS input voltage is given by the following equation:

$$V_{RMS} = \sqrt{\frac{1}{t}\int_{t}^{1+T} u^2(t)dt} = \frac{1}{N}\sqrt{\sum_{n=1}^{N} U^2(n)} \tag{19}$$

where T is the period of the rectified input voltage (see Fig. 7), Ts is sampling period, and N = T/Ts.

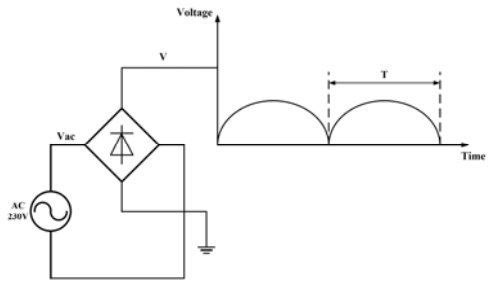

Fig. 7. The scheme for RMS input voltage calculation.

The block diagram of the PFC mode is shown in Fig. 8. The PFC is achieved by means of two cascade control loops. The outer voltage control loop maintains the voltage value in the DC intermediate circuit via a PI controller. The output of this controller, multiplied by the inverse squared V_{rms} and by V_{AC} forms the reference for the internal current control loop. The output of the current regulator triggers the PWM generator which generates the control for the MOSFET. The effect of the inclusion of the V_{AC} signal in the creation of the current reference consists in obtaining a form of current which copies the voltage form (with a certain scaling factor), thus the voltage and current signals go through zero at the same moments, providing an almost null phase shift and an almost uniform PF [16, 17].

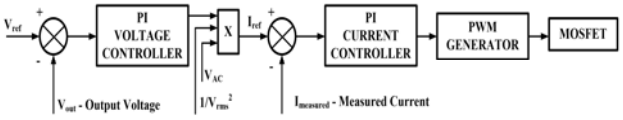

Fig. 8. Voltage and current controller block diagram.

The implementation in Matlab/Simulink of the PFC is presented in Fig. 9 and Fig. 10. The main parameters used in numerical simulation are: input voltage peak to the full bridge rectifier - Line_Voltage_Peak=230·sqrt(2)V; power line frequency - f_line=50Hz; desired output voltage from PFC Preconverter - V_{oref}= 400V; maximum steady state power capability - Power=100W; arbitrary resistive load - R=100Ω; arbitrary inductive Lm=0.001H; peak-peak output voltage ripple - del_V=10V; inductor current ripple - IndCurrRipple =8%; nominal efficiency of the preconverter - Conv_efficiency=92%; MOSFET switching frequency - f_sw= 50kHz; sampling time for the plant - T_s=1/(100·f_sw)sec; sampling time for the controller - T_{sc}=1/(50·f_sw)sec; proportional gain of the inner current loop controller K_p=0.093; integral gain of the of the inner current loop controller - K_i=1318; proportional gain of the outer voltage loop controller - K_p=0.115; integral gain of the of the outer voltage loop controller - K_i=21.75.

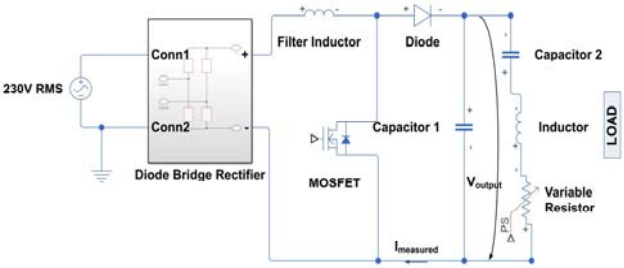

Fig. 9. PFC – Simulink implementation.

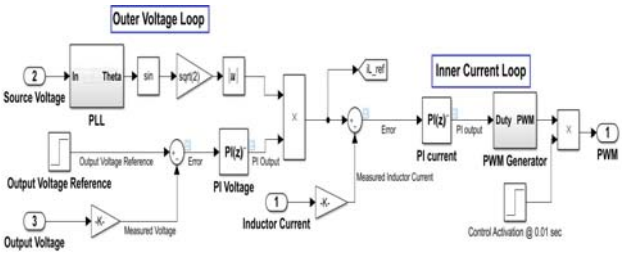

Fig. 10. Voltage and current controller for PFC – Simulink implementation.

For a load consisting of an RLC series circuit where R=100Ω, L=1mH, and C=100μF, the results of the numerical simulations are presented in Fig. 11 and Fig. 12. Fig. 12 shows the evolution of the current and voltage at the input of the PFC circuit, the voltage in the DC intermediate circuit and the evolution of the regulated current. The PFC circuit comes into operation after 10ms, thus, in Fig. 12 the PF is presented in the case of the presence of the PFC circuit, compared to the absence of the PFC circuit. It is noted that in the case of the presence of the PFC circuit, PF is about 1.

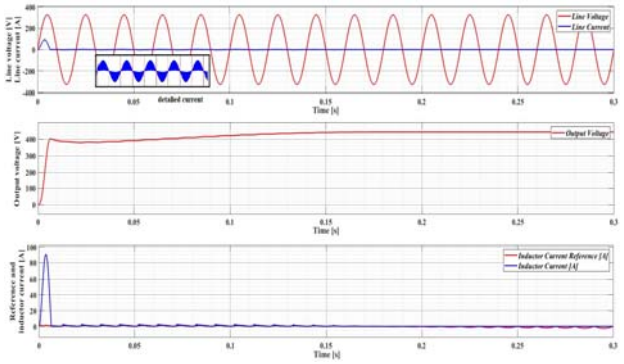

Fig. 11. Voltage and current waveforms – numerical simulation.

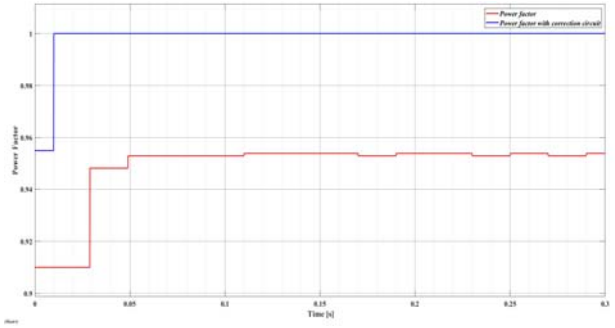

Fig. 12. PF comparison with and without correction circuit – numerical simulation.

V. Sensorless Control of PMSM

Fig. 13 presents a block diagram for the sensorless control of the PMSM based on the FOC strategy and power factor correction.

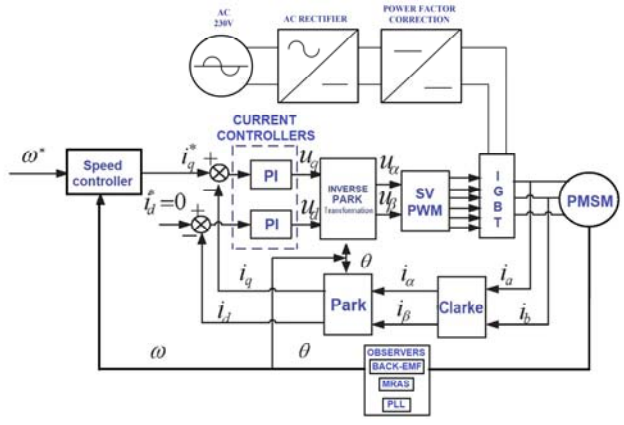

Fig. 13. Sensorless control of PMSM based on FOC strategy and PFC

The FOC control strategy consists in a cascade control system where the role of the outer loop is to adjust the speed. The references for the internal current control loop are prescribed by the speed controller for I_q, and I_d is set to zero for torque maximization [4]. The PFC was presented in previous section. The rotor position and speed estimation are achieved by means of observers. Three observers are presented next: the back-EMF sliding mode observer, the MRAS observer, and the PLL observer.

A. Back-EMF sliding mode observer

Based on the PMSM model, the current equations in α-β frame can be obtained by using inverse Park transformation, as follows:

$$\begin{aligned} \frac{di_\alpha}{dt} &= -\frac{R}{L}i_\alpha - \frac{1}{L}e_\alpha + \frac{1}{L}u_\alpha \\ \frac{di_\beta}{dt} &= -\frac{R}{L}i_\beta - \frac{1}{L}e_\beta + \frac{1}{L}u_\beta \end{aligned} \tag{20}$$

The back-EMF voltages are obtained in the following form:

$$\begin{aligned} e_\alpha &= \frac{d\psi_{m\alpha}}{dt} = -\lambda_0\omega_e \sin(\theta_e) \\ e_\beta &= \frac{d\psi_{m\beta}}{dt} = -\lambda_0\omega_e \cos(\theta_e) \end{aligned} \tag{21}$$

First it is necessary to estimate the back-EMF e_α and e_β for estimate the rotor speed. For this purpose, a sliding mode observer [22, 23] will be used, which is given by:

$$\begin{aligned} \frac{d\hat{i}_\alpha}{dt} &= -\frac{R}{L}\hat{i}_\alpha + \frac{1}{L}u_\alpha - \frac{l_1}{L}sign(\hat{i}_\alpha - i_\alpha) \\ \frac{d\hat{i}_\beta}{dt} &= -\frac{R}{L}\hat{i}_\beta + \frac{1}{L}u_\beta - \frac{l_1}{L}sign(\hat{i}_\beta - i_\beta) \end{aligned} \tag{22}$$

A sliding mode is enforced after a limited time if l1 > max (|eα |, |eβ|). By using the equations (12), errors are defined as $\bar{i}_\alpha = \hat{i}_\alpha - i_\alpha$ and $\bar{i}_\beta = \hat{i}_\beta - i_\beta$, and the following relations are obtained:

$$\begin{aligned} \frac{d\bar{i}_\alpha}{dt} &= -\frac{R}{L}\bar{i}_\alpha - \frac{1}{L}e_\alpha - \frac{l_1}{L}sign(\bar{i}_\alpha) \\ \frac{d\bar{i}_\beta}{dt} &= -\frac{R}{L}\bar{i}_\beta - \frac{1}{L}e_\beta - \frac{l_1}{L}sign(\bar{i}_\beta) \end{aligned} \tag{23}$$

When sliding mode occurs, the error is null thus $\bar{i}_\alpha = 0$ and $\bar{i}_\beta = 0$ and also: $\frac{d\bar{i}_\alpha}{dt} = 0$ and $\frac{d\bar{i}_\beta}{dt} = 0$.

The desired back-EMF quantities e_α and e_β are obtained by using the equivalent values of the switching quantities:

$$\begin{aligned} \left(l_1 sign(\bar{i}_\alpha)\right)_{eq} &= e_\alpha \\ \left(l_1 sign(\bar{i}_\beta)\right)_{eq} &= e_\beta \end{aligned} \tag{24}$$

The block diagram of the back-EMF sliding mode observer described is implemented in Simulink and is presented in Fig. 14.

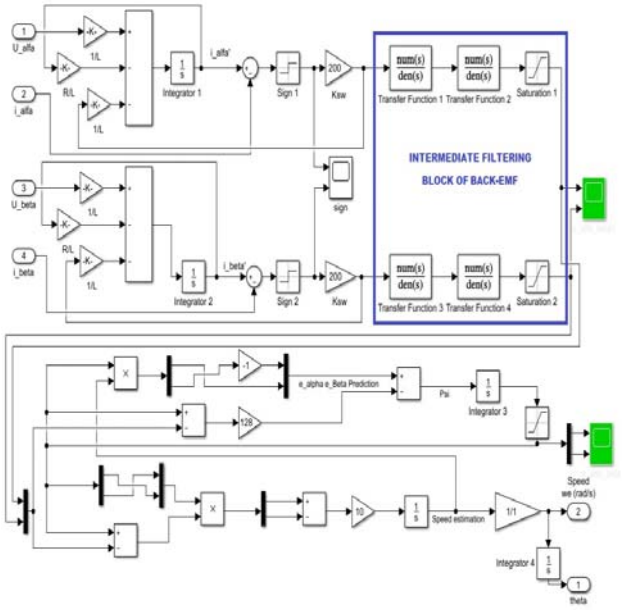

Fig. 14. Back-EMF and rotor speed sliding mode observer - Simulink implementation.

B. *MRAS observer*

Fig. 15 presents the block diagram of the MRAS. In the case where even the PMSM is the reference model, I_d and I_q currents can be acquired directly. For an adaptive model of PMSM described by an equation of the type (3), the Matlab/Simulink implementation is presented in Fig. 16. In this model, the values of the I_d and I_q currents are updating according to ω, the intermediate signal ξ is formed:

$$\xi(t) = i_d\hat{i}_q - i_q\hat{i}_d - \frac{\phi}{L}(i_q - \hat{i}_q) \tag{25}$$

To assure the convergence of the observer in the adaptation mechanism (see Fig. 17) a PI controller is inserted. Based on these, the rotor speed is estimated by:

$$\hat{\omega}(t) = k_p\xi(t) + \int_0^t k_i\xi(\tau)d\tau \tag{26}$$

where k_p and k_i, are the adjustment parameters of the PI controller. The stability of the observer is proved using the Popov hyperstability theory according to [24].

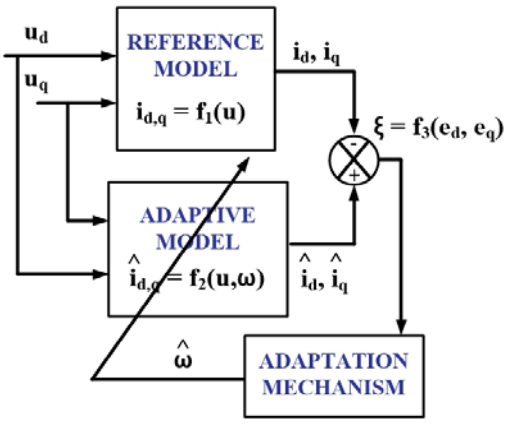

Fig. 15. Speed estimation scheme for MRAS.

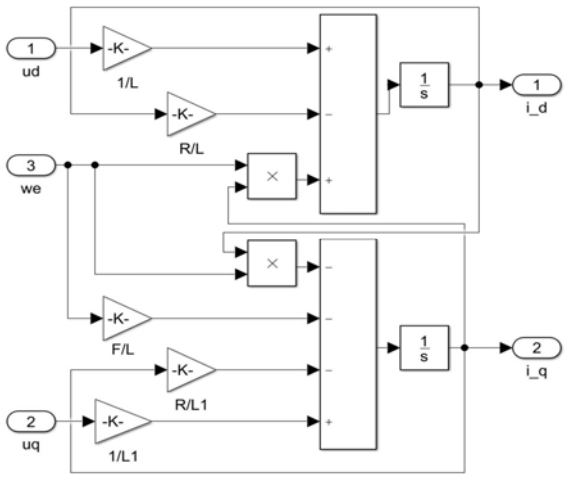

Fig. 16. Adaptive model for MRAS – Simulink implementation.

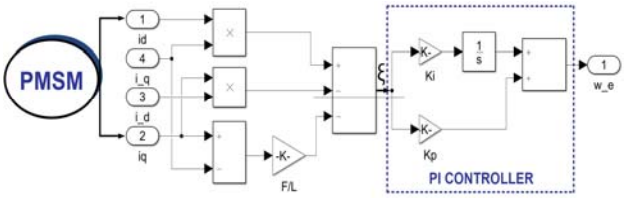

Fig. 17. Block diagram of the adaptation mechanism for MRAS – Simulink implementation.

C. *PLL observer*

For the PMSM supply system of the form:

$$\begin{cases} u_a = u\cos\omega_e t \\ u_b = u\cos(\omega_e t - 2\pi/3) \\ u_c = u\cos(\omega_e t + 2\pi/3) \end{cases} \tag{27}$$

the transformation matrix of three-phase voltage into d-q coordinate system is:

$$T(\hat{\theta}_e) = \frac{1}{3}\begin{bmatrix} \cos\hat{\theta}_e & \cos(\hat{\theta}_e - \frac{2\pi}{3}) & \cos(\hat{\theta}_e + \frac{2\pi}{3}) \\ \sin\hat{\theta}_e & -\sin(\hat{\theta}_e - \frac{2\pi}{3}) & -\sin(\hat{\theta}_e + \frac{2\pi}{3}) \end{bmatrix} \tag{28}$$

where $\hat{\theta}_e$ is the estimated phase angle of the output which is used by PLL observer, and $\hat{\theta}_e = \hat{\omega}_e t$.

The equation of the three phase stator winding of PMSM in the d-q coordinate system is:

$$\begin{bmatrix} u_d \\ u_q \end{bmatrix} = \begin{bmatrix} u\sin(\hat{\theta}_e - \theta_e) \\ u\cos(\hat{\theta}_e - \theta_e) \end{bmatrix} \tag{29}$$

Let $\overline{\theta}_e = \hat{\theta}_e - \theta_e$, the estimated error of the PLL. By imposing u_{dref} =0, the block diagram of the PLL observer is shown in Fig. 18 and the implementation in Simulink is shown in Fig. 19.

The convergence of the observer is achieved by using a PI controller, which allows the PLL estimation value to track the actual position of the rotor, and the error $\overline{\theta}_e$ is zero [13].

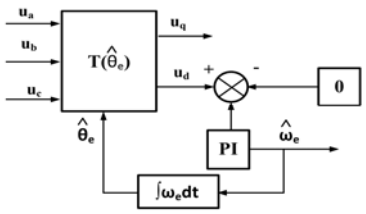

Fig. 18. Block diagram of rotor speed and position based on PI controller.

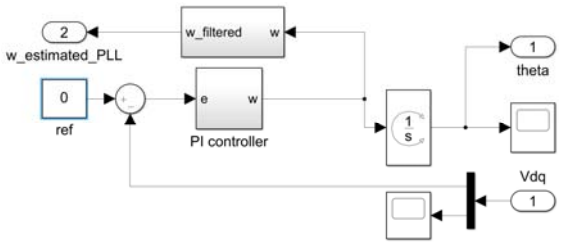

Fig. 19. PLL observer – Simulink implementation.

Further is presented the numerical simulations for sensorless control of an PMSM with the next nominal parameters: stator resistance R_s=2.875Ω; q and d inductance: L_q=L_d=0.0085H; combined inertia of rotor and load J=0.8e-3 kg·m^2; combined viscous friction of rotor and load B=0.005N·m·s/rad; induced flux by the permanent magnets of the rotor in the stator phases λ_{af}=0.175Wb; and pole pairs number P=4. The observers used for speed estimation were presented above. The adjustment parameters of the PI type speed controller of the FOC strategy are K_p=1 and K_i=50. The adjustment parameters of the PI controllers for the MRAS and PLL observers in the numerical simulations presented are: K_{p_MRAS}=80 and K_{i_MRAS}=15; K_{p_PLL}=3 and K_{i_PLL}=800.

The transfer function of the each PI controller is given by:

$$H_{PI}(s) = K_p + K_i \frac{1}{s} \tag{30}$$

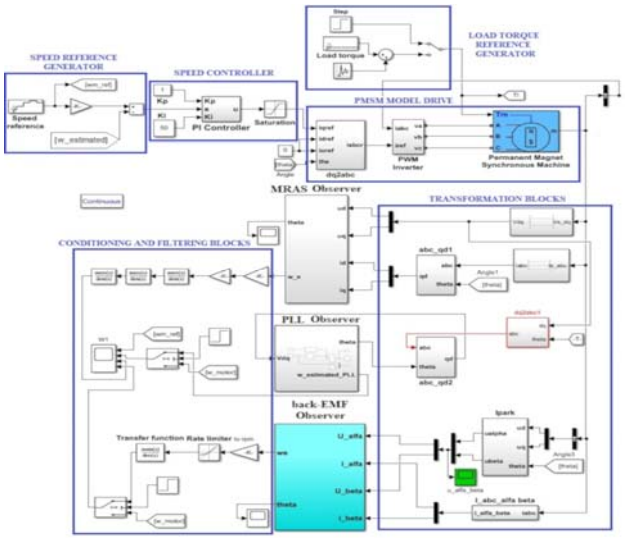

Fig. 20. Sensorless control of PMSM based on FOC strategy and comparison between back-EMF, MRAS, and PLL observers – Simulink implementation.

Due to the fact that starting of a PMSM motor in the sensorless type is a special one (it starts from a position stored from the previous start, or the control is achieved in open loop after a predefined sequence), in the achieved simulation, for the first 100ms, the output of the observers is bypassed.

The block diagram of the implementation in Matlab/Simulink for sensorless control of the PMSM based on the FOC strategy is presented in Fig. 20.

The time evolution of the comparison between the reference speed, the PLL speed estimation and the MRAS speed estimation is shown in Fig. 21. It is noted that the responses of MRAS and PLL type observers are slightly oscillating and characterized by overshooting.

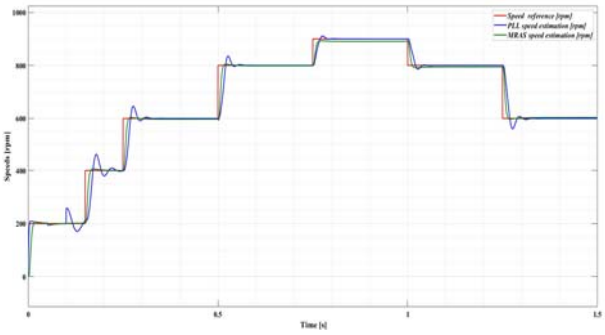

Fig. 21. Time evolution of the reference speed, PLL speed estimation, and MRAS speed estimation.

The time evolution of the quantities provided by the back-EMF sliding mode observer described is presented in Fig. 22. After applying a 300rpm step signal, the sliding mode observer accurately estimates the speed and position of the rotor. Also Fig. 22 presents the estimated back-EMF e_α, e_β, and I_d and I_q currents. The global PMSM control strategy used in this case is of FOC type, and in Fig. 22 this is reflected by the fact that the I_d current reference is set to 0, the I_d current having an oscillating evolution around this value. For the next speed reference sequence: [0 0.45]s→[300 600]rpm, the acceleration for speed ramps by 600rpm/s and 0.1Nm load torque reference, the results of the time evolution simulation of the sensorless control of PMSM with back-EMF sliding mode observer are presented in Fig. 23. The elements shown are: speed reference, rotor speed, load and electromagnetic torque, stator currents $I_{s\_a,b,c}$ and stator voltage $V_{s\_d,q}$. It is noticed that the system behaves with good results without overshooting, with response and very small rising time.

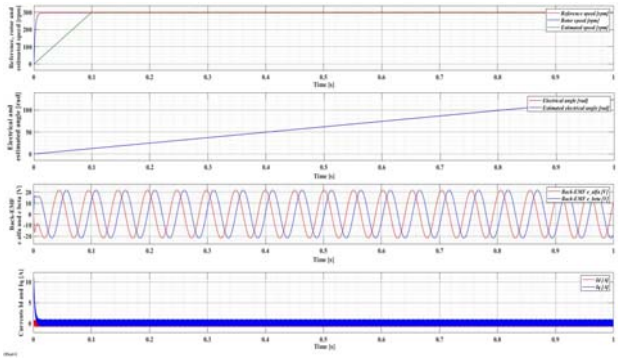

Fig. 22. Time evolution simulation of back-EMF, rotor position and rotor speed estimation based on back-EMF sliding mode observer.

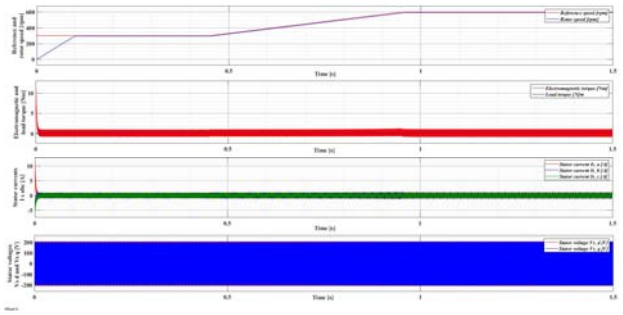

Fig. 23. Time evolution simulation of sensorless control of PMSM based on FOC strategy and back-EMF sliding mode observer.

Very good speed estimation is noticed as compared to MRAS and PLL observers, but at the same time it is noted that the structure of the back-EMF sliding mode observer is much more complex than the structure of the other two observers. This will result in choosing a medium/high performance DSP for implementation in an embedded system of the back-EMF observer. For the implementation of the PMSM and PFC sensorless control in the same embedded system, in future approaches it is suggested to use the CLA (Control Law Acceleration) type of DSPs with an additional control and execution unit, while the FOC sensorless control strategy will be implemented in the main DSP, and the PFC controller will be implemented in the CLA.

VI. Sensorless Control of PMSM Hardware and Software Implementattion

For the implementation in an embedded system of the sensorless control system using the FOC strategy, the DRV8312-EVM development hardware platform was selected. This is intended for the control of the PMSM/BLDC motors.

The main features of this development hardware platform are: max input voltage - 52.5V DC; max continuous output current per phase - 3.5A and a current peak - 6.5A; driver switching frequency - up to 500kHz; power supply including on-board regulation for powering additionally circuits - 24V; isolated CAN and SPI communication; closed-loop digital control with feedback using the C2000's family microcontrollers, on-chip PWM and ADC peripherals; on-board isolated JTAG emulation through the SCI peripheral; quadrature encoder interface; Hall sensor interface; high performance ADC; high precision voltage reference chip; three PWM DAC's generated by low pass filtering; and over current protection on the inverter stage [25-28].

The microcontroller F28069 Piccolo runs software programs from the C28x family, which is a member of the TMS320C2000 MCU platform. The F28069 Piccolo microcontroller provides high performance by including the CLA (Control Law Accelerator) device, connected with the control modules to the peripheral devices. The main features of this microcontroller are: frequency - 90 MHz (11.11-ns Cycle Time); MAC operation - multiply and accumulate 16×16 and 32×32 respectively; Harvard Bus Architecture; Fast Interrupt Response; Unified Memory Programming Model; Code-Efficient (in C/C++ and Assembly); Programmable Control Law Accelerator (CLA) which executes Code Independently of the Main CPU and 32-Bit Floating-Point Math Accelerator; up to 256KB of flash memory and up to 100KB RAM memory; 6-Channel Direct Memory Access (DMA); up to 8 Enhanced Pulse-Width Modulator (ePWM) and 16 PWM Channels Total (8 HRPWM-Capable); independent 16-Bit Timer in each module; 12-Bit Analog-to-Digital Converter (ADC); two Serial Peripheral Interface (SPI) Modules; and one Inter-Integrated-Circuit (I2C) Bus [28].

The development of the PMSM control application is carried out in Simulink, by using C28x peripheral blocks and blocks of the C28x DMC library (Motor Digital Control) in the Embedded Coder Support package for Texas Instruments C2000 processors. The generation of the executable code is carried out through the RTW Simulink, which will transfer the object code to the Code Composer environment. This way, all the features of this integrated development environment can be used, such as the download of the program into the F28069 Piccolo microcontroller, the control of execution and the debug function [28].

Fig. 24 presents the implementation in Simulink of closed-loop FOC algorithm.

The implementation of the FOC control algorithm in this example uses asynchronous programming. The pulse width modulation block (PWM) triggers ADC conversion, and at the end of the conversion, the ADC provides an interrupt triggering the main FOC algorithm.

The C28x hardware interrupt block deals with the issue of external interrupts, allowing for asynchronous processing, and triggers the execution of capture modules eCAP1, eCAP2, eCAP3 and CLATask1. The capture modules are achieved based on Function-Call subsystems which run when an event occurs. The eCAP blocks are used in this application for each capture pin from Hall A, B, and C sensors. In APWM mode, pins are used to generate PWM commands. The data storage block defines and initializes a shared data location, which is a memory region which can be used for reading or writing [27].

The Clarke-Park and SVPWM transformation blocks are shown in Fig 25. Also, in the case of the sensorless control, Fig. 25 presents a speed sliding mode observer.

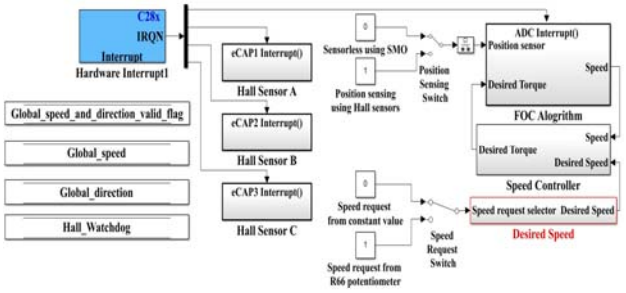

Fig. 24. Implementation in Simulink of closed-loop FOC algorithm.

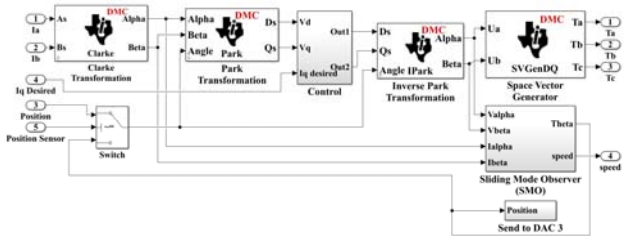

Fig. 25. Implementation in Simulink of Clarke-Park transformation, current controllers, SVPWM and speed sliding mode observer.

As described in Section 3, it is first necessary to identify the PMSM parameters before running the previously presented control program. For this operation the InstaSPIN-FOC graphical user interface will be used.

By sequentially following the steps for the determination of the PMSM parameters in Section 3 (where the motor was simulated by the operating equations), however in the case of a PMSM DT4260 type motor with the nominal parameters mentioned in Table 1. It can be seen that the results obtained in Fig. 26 and Fig. 27 regarding the online estimation of PMSM parameters are in agreement with the results obtained offline by numerical simulations in Section 3.

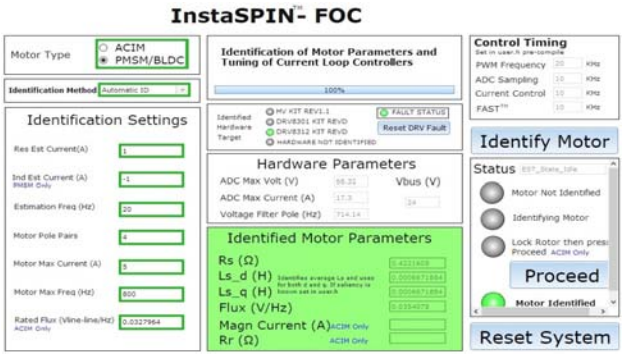

Fig. 26. Online identification of PMSM electrical parameters.

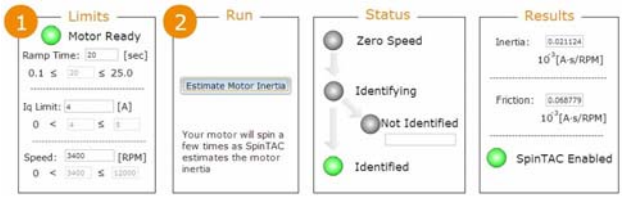

Fig. 27. Online identification of PMSM mechanical parameters.

It is noted that the parameters mentioned in Table 1, calculated by numerical simulation match the parameters identified online. For example, nominal R_s is 0.405Ω, R_s obtained from numerical simulation is 0.41Ω, and 0.42Ω was obtained by online identification.

Fig. 28 shows the evolution of the PMSM speed after the application of a speed reference of 5000rpm (1200rpm/s acceleration), of the currents I_d and I_q and the load torque. A detail of the speed evolution is shown in Fig. 29.

Fig. 28. Real time evolution of rotor speed, $I_{d,q}$ currents, and electromagnetic torque of PMSM.

The images of the experimental test for the sensorless control of the PMSM with DRV8312-EVM development hardware platform are presented in Fig. 30 and Fig. 31.

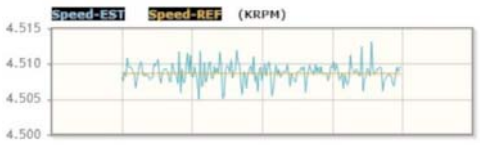

Fig. 29. Real time evolution of rotor speed of PMSM - detail.

Fig. 30. Image of the experimental test.

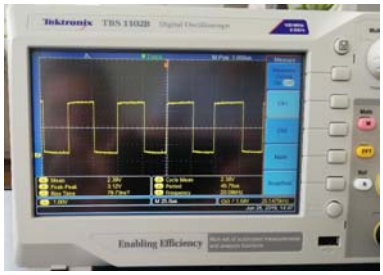

Fig. 31. PWM channel A - waveform on the scope.

VII. Conclusions

This article presents an identification procedure of the parameters and a sensorless control of a PMSM based on the FOC strategy and PFC. The proposed procedure for identifying the electrical and mechanical parameters of the PMSM is required in industrial applications at the beginning of a drive cycle due to variations of these parameters with the temperature, or in the event that the motor's parameters are unknown. The parameter identification procedure is implemented in the Matlab/Simulink environment. This procedure was also implemented in an embedded system and the results of the offline and online identification methods of the nominal parameters of the PMSM are presented comparatively to the parameters in the datasheet.

It presents the block structure of the PFC together with the numerical simulations achieved in Matlab/Simulink, on the improvement of the PF of the supply circuit. It also presents the block structures of the FOC strategy and of the back-EMF sliding mode, MRAS, and PLL type observers. The numerical simulations show the superiority of rotor speed estimation when using the back-EMF sliding mode observer compared to the rotor speed estimate provided by MRAS and PLL observers. This can also be explained by the less complex structure of MRAS and PLL observers compared to the structure of the back-EMF sliding mode observer.

The hardware and software implementation for a sensorless control PMSM using the FOC strategy and the speed back-EMF sliding mode observer is also presented. Results are presented for the PMSM control in real time using an embedded system. Although the selected embedded system is of low/medium cost type, it allows for a relatively large number of arithmetic operations to be implemented in real time due to both the FOC control strategy and especially the speed back-EMF observer. Future works will approach the implementation of Kalman type observers (requiring very complex real-time operations) to test the capabilities of a low/medium cost embedded system in terms of the PMSM control and the implementation in an embedded system of a PFC and sensorless control of a PMSM based on the FOC strategy, by using the DSPs with an additional control and execution unit - CLA.

ACKNOWLEDGMENT

The paper was developed with funds from the Ministry of Research and Innovation as part of the NUCLEU Program: PN 19 38 01 03.

Contribution of authors:
First author – 40%
First coauthor – 40%
Second coauthor – 10%
Third coauthor – 5%
Fourth coauthor – 5%

Received on October 2, 2019
Editorial Approval on November 25, 2019

REFERENCES

[1] M. Abassi, A. Khlaief, O. Saadaoui, A. Chaari, and M. Boussak, "Performance analysis of FOC and DTC for PMSM drives using SVPWM technique," *16th International Conference on Sciences and Techniques of Automatic Control and Computer Engineering (STA)*, Monastir, Tunisia, 2015, pp. 228-233.

[2] P. Siwek and K. Urbanski, "Improvement of the Torque Control Dynamics of the PMSM Drive Using the FOC-Controlled Simple Boost QZSDMC Converter," *23rd International Conference on Methods & Models in Automation & Robotics (MMAR)*, Miedzyzdroje, Poland, 2018, pp. 29-34.

[3] L. Yu, C. Wang, H. Shi, R. Xin, and L. Wang, "Simulation of PMSM field-oriented control based on SVPWM," *29th Chinese Control And Decision Conference (CCDC)*, Chongqing, China, 2017, pp. 7407-7411.

[4] B. K. Bose, Modern power electronics and AC drives, Prentice Hall, Knoxville, Tennessee, USA, 2002.

[5] P. C. Krause, O. Wasynczuk, and S. D. Sudhoff. Analysis of Electric Machinery and Drive Systems. IEEE Press, 2002.

[6] A. Fezzani, S. Drid, A. Makouf, L. Chrifi-Alaoui, and M. Ouriagli, "Speed Sensoless Robust Control of Permanent Magnet Synchronous Motor Based on Second-Order Sliding-Mode Observer," in Serbian Journal of Electrical Engineering (SJEE), vol. 11, no. 3, pp. 419-433, October 2014.

[7] B. Liu, " Speed control for permanent magnet synchronous motor based on an improved extended state observer," in Advances in Mechanical Engineering, vol. 10, no. 1, pp. 1-12, January 2018.

[8] X. Liu, G. Zhang, L. Mei, and D. Wang, "Speed estimation and Parameters Identification simultaneously of PMSM based on MRAS," in WSEAS Transactions on Systems and Control, vol. 12, no. 1, pp. 183-192, December 2017.

[9] X. Wu, H.Wang, X. Yuan, S. Huang, and D. Luo, "Design and Implementation of Recursive Model Predictive Control for Permanent Magnet Synchronous Motor Drives," in Mathematical Problems in Engineering, vol. 2015, pp. 1-10, April 2015.

[10] M. Nicola, C. I. Nicola, and M. Duță, "Adaptive Sensorless Control of PMSM using Back-EMF Sliding Mode Observer and Fuzzy Logic," *The Electric Vehicles International Conference (EV)*, Bucharest, Romania, 2019, pp 1-6.

[11] M. Nicola, C. I. Nicola, and A. Vintilă, "Sensorless Control of Multi-Motors PMSM using Back-EMF Sliding Mode Observer," *The Electric Vehicles International Conference (EV)*, Bucharest, Romania, 2019, pp 1-6.

[12] H. Tang, H. Li, and J. Lin, "Research on Sensorless Control Method of PMSM Based on a Kalman Filter Sliding Mode Observer," *10th International Conference on Measuring Technology and Mechatronics Automation (ICMTMA)*, Changsha, China, 2018, pp. 290-293.

[13] X. Ren, M. Wang, and J. Chen, "Rotor Position and Velocity Estimation of SMO Based on PLL," *2nd International Conference on Mechanical, Electronic, Control and Automation Engineering (MECAE)*, Qingdao, China, 2018, pp. 243-248.

[14] J. Zambada and D. Deb, Sensorless Field Oriented Control of PMSM Motors – Aplication Note 1078, Microchip Technology Inc., 2010.

[15] C. I. Nicola, M. Nicola, S. Popescu, and M. Duta, "Power Factor Correction and Sensorless Control of PMSM Using FOC Strategy," *12th International Conference and Exhibition on Electromechanical and Energy Systems (SIELMEN)*, Chi□inău, Moldova, 2019, pp. 329-334.

[16] Texas Instruments, Digital Control of Two Phase Interleaved PFC and Motor Drive Using MCU With CLA, Appl. Report SPRABS5, 2013.

[17] Texas Instruments, Two-Phase Interleaved PFC Converter Power Metering Test Results, Appl. Report TIDU249, 2014.

[18] J. Long, M. Yang, Y. Li, Y. Chen, and D. Xu, "Parameter identification of permanent magnet synchronous motors: Sequence strategy comparative study," *IEEE Transportation Electrification Conference and Expo, Asia-Pacific (ITEC Asia-Pacific)*, Harbin, China, 2017, pp. 1-6.

[19] C. I. Nicola, M. Nicola, A. Vintilă, and D. Sacerdo□ianu, "Identification and Sensorless Control of PMSM Using FOC Strategy and Implementation in Embedded System," *12th International Conference and Exhibition on Electromechanical and Energy Systems (SIELMEN)*, Chisinau, Moldova, 2019, pp. 335-340.

[20] Mathworks, *Simscape Electrical User's Guide*, The MathWorks, Inc., 2019.

[21] H. W. Sim, J.S. Lee, and K. B. Lee, "On-line Parameter Estimation of Interior Permanent Magnet Synchronous Motor using an Extended Kalman Filter", in Journal of Electrical Engineering and Technology, vol. 9, no. 2, pp. 600-608, March 2014.

[22] V. Utkin, J. Guldner, and J. Shi, Sliding mode control in electromechanical systems, second edition. Automation and Control Engineering, Taylor & Francis, 2009.

[23] A. S. Mohamed, M. S. Zaky, A. S. Din, and H. Yasin, "Comparative Study of Sensorless Control Methods of PMSM Drives," in Innovative Systems Design and Engineering, vol. 2, no. 5, pp. 44-66, November 2011.

[24] J. Zambada and D. Deb, Sensorless Field Oriented Control of PMSM Motors, Appl. Note 1078, Microchip Technology Inc., 2010.

[25] A. Samar, P. Saedin, A. I. Tajudin, and N. Adni, "The implementation of Field Oriented Control for PMSM drive based on TMS320F2808 DSP controller," *IEEE International Conference on Control System, Computing and Engineering*, Penang, Malaysia, 2012, pp. 612-616.

[26] H. Mehta, V. Joshi, and P. Kurulkar, "Implementation issues of sliding mode observer for sensorless field oriented control of PMSM using TMS320F2812," *IEEE Symposium on Sensorless Control for Electrical Drives (SLED)*, Nadi, Fiji, 2016, pp. 1-6.

[27] H. A. Toliyat and S. Campbell, DSP-Based electromechanical motion control. CRC Press, 2004.

[28] V. S. Kumari, R. Anil kumar, S. S. Nawaz, "Speed Control of BLDC Motor using DRV8312EVM in VisSim Environment", in CVR Journal of Science and Technology, vol. 14, pp. 43-48, June 2018.